DESIGNING RANDOM FM RADAR WAVEFORMS WITH COMPACT SPECTRUM

Charles A. Mohr[1,2], *Shannon D. Blunt*[2]

[1]Sensors Directorate, Air Force Research Laboratory (AFRL), Wright-Patterson AFB, OH
[2]Radar Systems Lab (RSL), University of Kansas, Lawrence, KS

ABSTRACT

Spectrally-shaped random FM (RFM) waveforms have recently been shown to greatly expand radar design freedom, provide good spectral containment, and are amenable to physical implementation in high-power transmitters. A key design factor involves ways of enforcing a Gaussian spectral density via optimization, which leads to a Gaussian autocorrelation that theoretically has no range sidelobes. However, the gradual roll-off for this spectrum means that, for fixed transmitter bandwidth, the passband component must be narrower than for classical linear FM (LFM), thereby trading achievable range resolution. Here we examine the impact of using the family of super-Gaussian spectra to serve as alternative design templates. Using the temporal template error (TTE) RFM design scheme to generate physical waveforms in this context, radar performance trade-offs are examined to assess practical viability.

Index Terms—radar waveform agility, noise radar

1. INTRODUCTION

The class of *noise radar* waveforms, in which the transmitted signal is literally random noise, has been around for quite some time and received considerable attention (e.g. [1-4]). Just as old, but less widely known, is the sub-class of frequency modulated (FM) noise, or random FM (RFM), [5-8]. Where the broad class is limited to short-range applications since true noise exhibits significant amplitude modulation (AM), the latter sub-class realizes waveforms that are constant amplitude and continuous, thereby enabling use in high-power transmitters and long-range applications.

Early work on RFM was driven by white noise, realizing spectral densities whose associated autocorrelations tend to have high range sidelobes (see [9]). It has recently been shown [10,11] that imposing structure to RFM can provide a Gaussian spectral density in the expectation (over the set of unique waveforms), yielding a per-waveform peak sidelobe level (PSL) of ~$10\log_{10}(B_{3\text{dB}}T)$ after expectation, for 3-dB bandwidth $B_{3\text{dB}}$ and pulse width T. Better sidelobe performance can be achieved by optimizing each waveform to match the desired spectrum density (e.g. [12-17]).

Another factor for all nonrepeating waveforms that is distinct from classical radar operation arises when performing slow-time (Doppler or cross-range) processing after pulse compression. For L pulses in the coherent processing interval (CPI), RFM waveforms incur an additional $10\log_{10}(L)$ factor of range sidelobe suppression due to incoherent averaging, while the autocorrelation mainlobes still combine coherently for SNR gain. There is a range sidelobe modulation (RSM) of the clutter that also arises during slow-time processing, though a variety of methods have been developed to address it [12,18].

Here our focus is on maximizing usage of fixed spectral content, such as imposed by the transmitter or a regulatory mask [19]. The LFM waveform represents the practical extreme in spectral containment, since it approximates the theoretical (yet physically unachievable) rectangular shape, though it's repeated use over the CPI results in a PSL of about 13 dB. In contrast, RFM waveform sets comprising 10,000 unique waveforms have been experimentally demonstrated in hardware (loopback and open-air) to achieve PSL values better than 70 dB, though the spectral footprint can be triple that of LFM to provide the same 3-dB bandwidth.

To explore a middle ground between these extremes, we examine the use of super-Gaussian distributions [20] as spectral density templates, thus enabling tuning of the degree of sidelobe roll-off. We evaluate the resulting performance trade-off and then incorporate this tunable structure into a particular RFM waveform optimization approach that has yielded good results in experimental measurements. The use of FM-appropriate optimal mismatched filtering (MMF) is also shown to partially compensate for this trade-off.

2. SUPER-GAUSSIAN SPECTRAL TEMPLATES

The super-Gaussian function is well known in optics [20] as a way to control the shape of a light beam. It is defined as

$$f(x) = A\exp\left(-\frac{1}{2}\left|\frac{(x-\gamma)}{\sigma}\right|^{n}\right), \qquad (1)$$

where σ and n are real and positive, A is an arbitrary real constant, and the function is centered at γ. Setting $n = 2$ realizes the standard Gaussian distribution, of which (1) is a particular generalization. Fig. 1 illustrates peak-normalized versions of (1) for different values of n and for $\gamma = 0$, with the value of σ in each case set such that the four functions cross at a point 35 dB below the peak, which corresponds to a normalized frequency of ±0.4. For $n = [2, 4, 16, 100]$, the

This work was supported by the Office of Naval Research under Contract #N00014-20-C-1006. DISTRIBUTION STATEMENT A. Approved for Public Release.

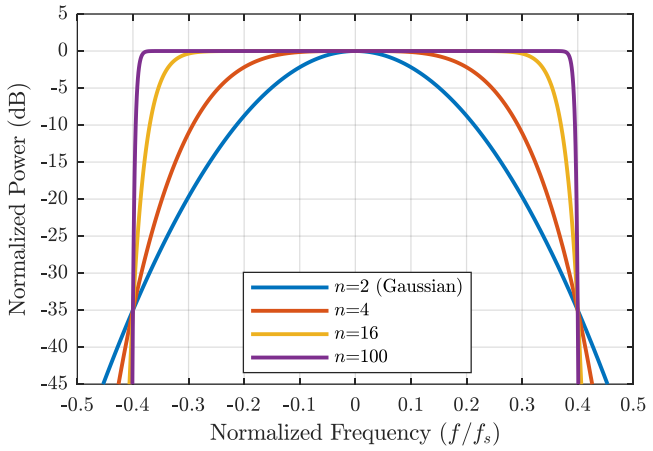

Fig. 1. Super-Gaussian spectral density templates for different n in (1), where f_s is the sample rate

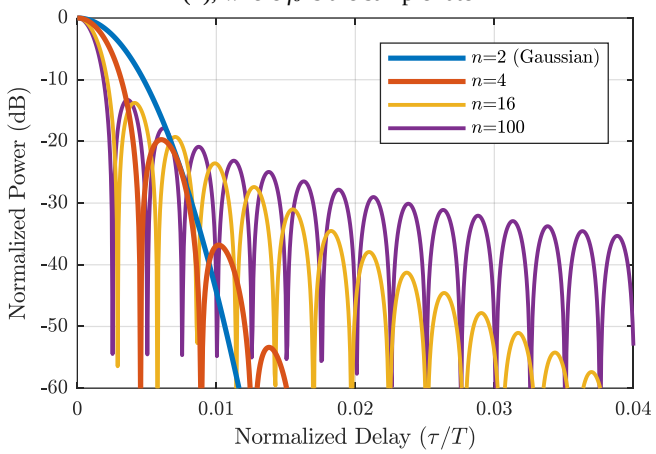

Fig. 2. Autocorrelations for the spectral density templates in Fig. 1

corresponding values of σ are approximately $\sigma = [2\times10^{-2}, 3\times10^{-3}, 5\times10^{-8}, 2\times10^{-41}]$.

As n increases in Fig. 1, the passband becomes flatter and the spectral roll-off steeper. For a radar transmitter with some maximum operational bandwidth, this trend means the 3-dB waveform bandwidth can be greater, thus achieving finer range resolution. Moreover, high-power transmitters impart both linear and nonlinear effects upon a waveform, with the latter mainly due to the high-power amplifier (HPA) being operated in saturation. The constant-amplitude and phase-continuous structure of FM is well-suited to this application, since the instantaneous frequency is only a single value, thus preventing intermodulation effects in the HPA. However, excessive roll-off also produces a filtering effect by the linear part of the transmitter, thereby inducing a deviation from FM and, somewhat counterintuitively, a *spectral regrowth* effect due to HPA intermodulation that can violate regulatory masks. It is for this reason that polyphase codes are not directly implemented at high power (see [21]).

A useful metric in this context is spectral efficiency of the waveform design template. Noting that design is performed on a discretized version of the FM waveform, the total design bandwidth is defined by sampling rate f_s. The portion allocated to waveform design thus defines spectral efficiency as

$$\Gamma_{\text{eff}} = B_{3\text{dB}} / f_s \,. \tag{2}$$

For the n = 2, 4, 16, and 100 templates in Fig. 1, the spectral efficiencies are approximately 0.23, 0.43, 0.69, and 0.80, respectively. These values are also the inverse of "over-sampling" factor K when performing optimization of discretized FM waveforms [12-17].

It is useful to also consider the waveform autocorrelation (i.e. matched filter response) associated with each spectral density via inverse Fourier transform. Fig. 2 illustrates these for the same cases as Fig. 1. The differences in $B_{3\text{dB}}$, and thus spectral efficiency, is clearly evident in Fig. 2 via the change in mainlobe width. However, since bandwidth can always scale, the more significant distinction arises from the change in sidelobe structure, with increasing n also corresponding to higher sidelobes. In fact, as $n \to \infty$ the autocorrelation (and PSL) essentially becomes the same as for LFM.

An important note here pertains to incoherent sidelobe averaging during slow-time processing. Because they correspond to a desired spectral template, RFM waveforms designed using cases like n = 4, 16, or 100 (or anything not strictly Gaussian) retain template-dependent range sidelobes that persist (i.e. do not average out). These persistent sidelobes require further consideration on receive.

2. RFM WAVEFORM DESIGN: TTE

To understand the practical implications of super-Gaussian spectral templates for RFM waveform design, we shall use the temporal template error (TTE) design approach recently developed in [15], which was demonstrated experimentally in loopback and with open-air measurements. The following serves as a brief review of TTE design.

Let $S(f)$ be the frequency representation of FM waveform $s(t)$, with the former defined as

$$S(f) = B(f)\exp(j\phi(f)) \,, \tag{3}$$

where $B(f)$ is a positive, real-valued spectral template and $\phi(f)$ is an arbitrary phase function. Therefore

$$s(t) = \mathcal{F}^{-1}\left\{B(f)\exp\left(j\phi(f)\right)\right\}, \tag{4}$$

for inverse Fourier transform $\mathcal{F}^{-1}\{\bullet\}$. Since $s(t)$ is a pulsed FM radar waveform it needs to possess finite time support and be constant amplitude. However, spectral shaping of an arbitrary phase function via (4) achieves neither requirement.

The TTE cost function [15] measures how far $s(t)$ in (4) is from meeting these pulsed and constant amplitude requirements by posing the squared-error metric

$$J = \int_0^T \left[\,|s(t)|^2 - u(t)\,\right]^2 dt \,, \tag{5}$$

where $u(t)$ is the pulse energy envelope (or temporal template) that is real and positive on interval $[0,T]$ and zero otherwise. The integral in (5) only extends over this interval even though some small amount of $s(t)$ will inevitably exist

outside $[0,T]$ after optimization. However, it is not necessary to extend the integral over $(-\infty,+\infty)$ as long as $u(t)$ and $s(t)$ are such that

$$\int_{-\infty}^{+\infty} u(t)\,dt = \int_{0}^{T} u(t)\,dt = \int_{-\infty}^{+\infty} |s(t)|^2\,dt\,. \tag{6}$$

Equation (6) defines $u(t)$ such that its total energy is confined to the interval $[0,T]$ AND is equivalent to the total energy of $|s(t)|^2$. Given these conditions on $u(t)$, (5) can be equal to zero if and only if all the energy of $|s(t)|^2$ is likewise concentrated in the interval [0,T], thus rendering integration from $(-\infty,\infty)$ in (5) unnecessary. Since $s(t)$ is defined in the frequency domain via (4), there is not a direct way to set the right-hand side of (6), though its frequency energy can be set through $B(f)$ and Parseval's theorem [22], such that

$$\int_{-\infty}^{+\infty} |S(f)|^2\,df = \int_{-\infty}^{+\infty} B^2(f)df = \int_{-\infty}^{+\infty} |s(t)|^2\,dt\,. \tag{7}$$

The goal of TTE optimization is thus to find phase function $\phi(f)$ whereby (5) is minimized given some random initialization. See [15] regarding proper discretization of (3)-(5) to ensure physically realizable waveforms. The design process is summarized in Table I, where $\boldsymbol{\phi}$ is the length $(2M-1)$ discretized version of $\phi(f)$, $\mathbf{s}$ and $\mathbf{u}$ are length-M discretized versions of $s(t)$ and $u(t)$, respectively, and $M = (B_{3\text{dB}}T)/\Gamma_{\text{eff}} = (B_{3\text{dB}}T)K$ ensures spectral roll-off is sufficiently captured to provide a high-fidelity representation of desired FM structure. Consequently, we can write (5) as

$$J(\boldsymbol{\phi}) = \left\| \bar{\mathbf{s}} \odot \bar{\mathbf{s}}^* - \bar{\mathbf{u}} \right\|_2^2 \tag{8}$$

$$\bar{\mathbf{s}} = \left[\mathbf{s}^T \quad \mathbf{0}_{1\times(M-1)} \right]^T \tag{9}$$

$$\bar{\mathbf{u}} = [\mathbf{u}^T \quad \mathbf{0}_{1\times(M-1)}]^T \tag{10}$$

for $\odot$ the Hadamard product, $(\bullet)^*$ denoting complex conjugation, and the length $(2M-1)$ discretization of (3) is

$$\mathbf{s}_{\text{f}} = \mathbf{b} \odot \exp(j\boldsymbol{\phi}), \tag{11}$$

where $\mathbf{b}$ is the discretization of $B(f)$. It is shown in [15] that the gradient of (8) with respect to $\boldsymbol{\phi}$ is

$$\mathbf{g} = \nabla_{\boldsymbol{\phi}} J(\boldsymbol{\phi}) = 4\Im\left\{ \mathbf{s}_{\text{f}}^* \odot \left[\mathbf{A}^H \left(\left\{ \bar{\mathbf{s}}^* \odot \bar{\mathbf{s}} - \bar{\mathbf{u}} \right\} \odot \bar{\mathbf{s}} \right) \right] \right\}, \tag{12}$$

where $\Im\{\bullet\}$ extracts the imaginary part of the argument and $\mathbf{A}^H$ applies the $(2M-1)\times(2M-1)$ discrete Fourier transform (DFT). Also note that (12) corrects conjugation and scale errors in [15].

The particular implementation in Table I is called heavy ball gradient descent, where simple backtracking sets the step size μ, and parameters $g_{\min}$, β, ρ_{up}, ρ_{down}, and c are specific to the particular gradient method [23,24]. Steps 3-13 comprise the gradient descent portion, while steps 14-16 account for the fact that optimization does not provide a phase function that perfectly matches the temporal template (i.e. (5) does not become identically zero). Consequently, (4) is applied to map the final optimized phase function into a discretized waveform (step 14), it is truncated to M samples (step 15), and then projected onto the constant-amplitude temporal template (step 16). This projection inevitably results in some small deviation from the desired spectrum, but optimization ensures it is negligible [15].

TABLE I: TTE OPTIMIZATION OF RFM WAVEFORMS

1:	**Initialize**: $M, \boldsymbol{\phi}_0, \mathbf{u}, \mathbf{b}, \mathbf{q}_0 = \mathbf{0}_{N\times 1}, g_{\min}, \beta, \mu, \rho_{\text{up}}, \rho_{\text{down}}, c,$ and set $i = 1$
2:	**Repeat**
3:	Evaluate: $J(\boldsymbol{\phi}_{i-1})$ and $\nabla_{\boldsymbol{\phi}} J(\boldsymbol{\phi}_{i-1})$ via (8) and (12)
4:	$\mathbf{q}_i = -\nabla_{\boldsymbol{\phi}} J(\boldsymbol{\phi}_{i-1}) + \beta \mathbf{q}_{i-1}$
5:	**If** $\left(\nabla_{\boldsymbol{\phi}} J(\boldsymbol{\phi}_{i-1})\right)^T \mathbf{q}_i \geq \mathbf{0}$
6:	$\mathbf{q}_i = -\nabla_{\boldsymbol{\phi}} J(\boldsymbol{\phi}_{i-1})$
7:	**End** (If)
8:	**While** $J(\boldsymbol{\phi}_{i-1} + \mu\mathbf{q}_i) > J_p(\boldsymbol{\phi}_{i-1}) + c\mu\left(\nabla_{\boldsymbol{\phi}} J(\boldsymbol{\phi}_{i-1})\right)^T \mathbf{q}_i$
9:	$\mu = \rho_{\text{down}}\,\mu$
10:	**End** (While)
11:	$\boldsymbol{\phi}_i = \boldsymbol{\phi}_{i-1} + \mu\mathbf{q}_i, \quad \mu = \rho_{\text{up}}\,\mu$
12:	$i = i + 1$
13:	**Until** $i = I$ **or** $\left\|\nabla_{\boldsymbol{\phi}} J(\boldsymbol{\phi}_i)\right\| < g_{\min}$
14:	$\tilde{\boldsymbol{s}} = \mathbf{A}(\mathbf{b} \odot \exp(j\,\boldsymbol{\phi}))$
15:	$\hat{\mathbf{s}} = [\tilde{\boldsymbol{s}}_1 \;\; \tilde{\boldsymbol{s}}_2 \cdots \;\; \tilde{\boldsymbol{s}}_M]^T$
16:	$\mathbf{s} = \mathbf{u} \odot \exp(j\angle\hat{\mathbf{s}})$

4. TTE DESIGN WITH SUPER-GAUSSIAN SPECTRA

To assess how well RFM waveforms can conform to super-Gaussian spectra, $L = 1000$ independent TTE waveforms were optimized for each case in Fig. 1. Discretized waveform length was set to $M = 1024$ samples, providing a waveform dimensionality trade-space via $M\Gamma_{\text{eff}} = B_{3\text{dB}}T$. Each phase function $\boldsymbol{\phi}$ was initialized with $(2M-1)$ independent draws from a uniform distribution on $[-\pi,+\pi]$. The gradient-descent parameters were $g_{\min} = 10^{-8}$, $\mu_0 = 10^{-4}$, $\beta = .98$, $\rho_{\text{up}} = 1.01$, $\rho_{\text{up}} = 0.9$, and $c = 10^{-2}$. Regardless of spectral template, each waveform optimization took about 3000 to 4000 iterations to reach the stopping criteria in step 13.

Fig. 3 shows that the average power spectra (over each 1000-waveform set) matches its template quite well. Here it is seen that the –35 dB cross-over point was chosen because that is the regime where template deviation tends to occur (based on previous observations), due to the spectrum aspect associated with the rectangular pulse envelope (i.e. a sinc function). Fig. 4 shows coherent slow-time autocorrelation combinations for each unique waveform set. Sidelobes well outside each mainlobe region are truly random, and thus combine incoherently to reach PSL values that are all at about –60 dB; close to a 30 dB improvement over the root-mean-square (RMS) autocorrelation for each case (dashed traces).

The difference between these spectral templates arises in and around each autocorrelation mainlobe (as expected from Fig. 2). Per the Fig. 4 inset, the n = 16 and 100 cases realize the narrowest mainlobe (at least for the top 10 dB or so), and exhibit a more gradual sidelobe roll-off thereafter (sometimes called *shoulder lobes* in this context). The n = 4 case has a similar result, though far less pronounced. Indeed, the value of $B_{3\text{dB}}T$ is determined to be 240, 443, 703, and 800 for n = 2, 4, 16, and 100, respectively. Thus, the n = 100 case realizes a physical FM waveform having $B_{3\text{dB}}$ that is more than triple that of the n = 2 case for the same T.

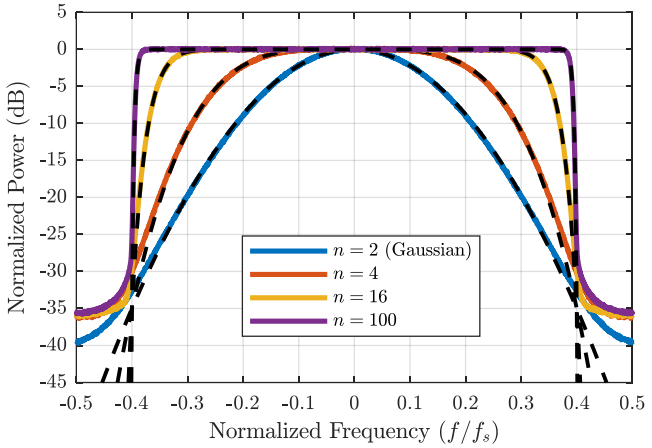

Fig. 3. Mean power spectrum for each unique set of 1000 TTE-optimized waveforms compared to its intended spectral template

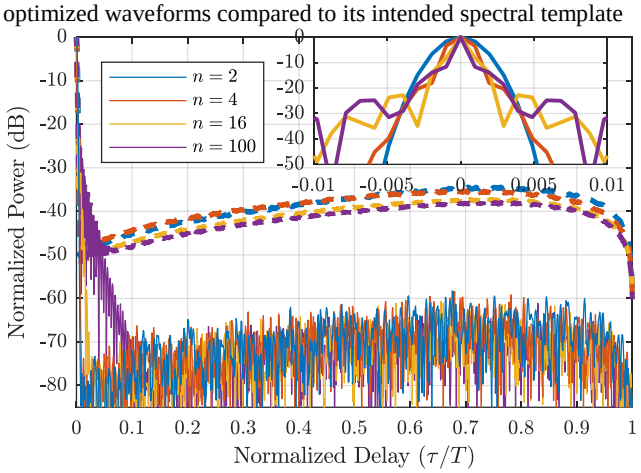

Fig. 4. Coherently combined (in slow-time) autocorrelations for each unique set of 1000 TTE-optimized waveforms, along with RMS autocorrelation responses (dashed traces)

5. SUPER-GAUSSIAN SIDELOBE MITIGATION

From a radar detection/false-alarm standpoint, shoulder lobes near the mainlobe (like Fig. 4) are not that detrimental. That said, there are methods to compensate, thereby further improving sensing performance. For instance, sidelobes for standard LFM are easily suppressed using amplitude windowing of the waveform's matched filter [25], which amounts to receive-only spectral shaping, though this simple MMF approach does sacrifice range resolution and incurs mismatch loss. Alternatively, a least-squares optimal MMF [26-28] has recently been developed for FM waveforms [12,29] and can be used to address these persistent sidelobes.

Per [12], an optimal MMF for the ℓth unique RFM waveform $\mathbf{s}_\ell$ can be determined via

$$\mathbf{h}_\ell = (\mathbf{S}_\ell^H \mathbf{S}_\ell + \delta\mathbf{I})^{-1}\mathbf{S}_\ell\mathbf{d}, \tag{13}$$

where

$$\mathbf{S}_\ell = \begin{bmatrix} \mathbf{s}_\ell & 0 & \cdots & 0 \\ 0 & \mathbf{s}_\ell & \ddots & \vdots \\ \vdots & \ddots & \ddots & 0 \\ 0 & \cdots & 0 & \mathbf{s}_\ell \end{bmatrix} \tag{14}$$

is an $(\tilde{M}+M-1)\times\tilde{M}$ banded Toeplitz matrix, $\delta\mathbf{I}$ is a $\tilde{M}\times\tilde{M}$ scaled identity matrix to prevent ill-conditioning, and $\mathbf{d}$ is a length $(\tilde{M}+M-1)$ vector containing the desired filter response. The MMF has length $\tilde{M} > M$ to provide more degrees of freedom for sidelobe suppression at the expense of greater sidelobe extent in range. Here $\mathbf{d}$ was chosen to be the autocorrelation corresponding to a Gaussian spectrum with the same 3-dB bandwidth as the respective waveform's spectrum, such that the MMF retains the same range resolution while ideally removing the shoulder sidelobes. An MMF was separately determined for each RFM waveform in each of the four sets. The resulting filter responses in Fig. 5 demonstrate roughly 10 dB further sidelobe suppression for both RMS and coherent combining further away from the mainlobe (compared to Fig. 4). More modest improvement is observed for shoulder lobe suppression, with the n = 100 case realizing about 7 dB suppression for the closest sidelobe.

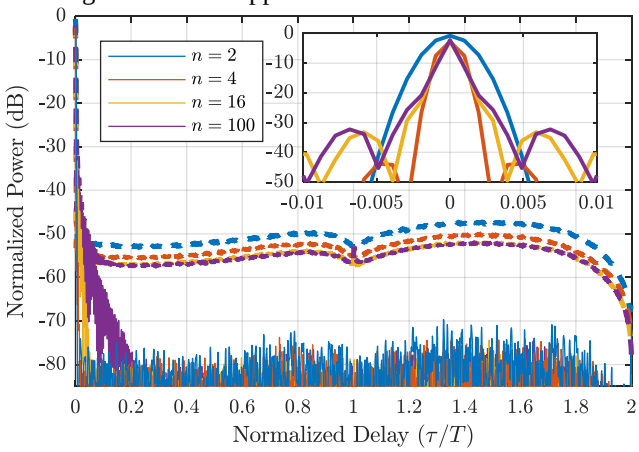

Fig. 5. Coherently combined (in slow-time) MMF responses for each unique set of 1000 TTE-optimized waveforms, along with RMS responses (dashed traces)

6. CONCLUSIONS

The key advantage of the Gaussian spectral template is that it has no persistent sidelobes. The super-Gaussian cases trade some degree of persistent shoulder lobes for better spectral efficiency (sharper roll-off), which translates into finer range resolution. These shoulder lobes can be partially suppressed via optimized mismatched filtering.

7. REFERENCES

[1] B.M. Horton, “Noise-modulated distance measuring systems,” *Proc. IRE*, vol. 47, no. 5, pp. 821-828, May 1959.

[2] X. Xu, R.M. Narayanan, “Range sidelobe suppression technique for coherent ultra wide-band random noise radar imaging,” *IEEE Trans. Antennas & Propagation*, vol. 49, no. 12, pp. 1836-1842, Dec. 2001.

[3] K. Lukin, A. Stove, C. Wasserzier, “Noise radar special issue – part 1,” *IEEE Aerospace & Electronic Systems Mag.*, vol. 35, no. 9, Sept. 2020.

[4] K. Lukin, A. Stove, C. Wasserzier, “Noise radar special issue – part 2,” *IEEE Aerospace & Electronic Systems Mag.*, vol. 35, no. 10, Oct. 2020.

[5] T.B. Whiteley, D.J. Adrian, “Random FM autocorrelation fuze system,” U.S. Patent #4,220,952, issued Sept. 2, 1980, application filed Feb. 17, 1956.

[6] L. Guosui, G. Hong, Z. Xiaohua, S. Weimin, “The present and future of random signal radars,” *IEEE Aerospace & Electronic Systems Mag*., vol. 12, no. 10, pp. 35-40, Oct. 1997.

[7] S.R.J. Axelsson, “Noise radar using random phase and frequency modulation,” *IEEE Trans. Geoscience & Remote Sensing*, vol. 42, no. 11, pp. 2370-2384, Nov. 2004.

[8] L. Pralon, B. Pompeo, J.M. Fortes, “Stochastic analysis of random frequency modulated waveforms for noise radar systems,” *IEEE Trans. Aerospace & Electronic Systems*, vol. 51, no. 2, pp. 1447-1461, Apr. 2015.

[9] S.D. Blunt, J.K. Jakabosky, C.A. Mohr, P.M. McCormick, J.W. Owen, B. Ravenscroft, C. Sahin, G.D. Zook, C.C. Jones, J.G. Metcalf, T. Higgins, “Principles and applications of random FM radar waveform design,” *IEEE Aerospace & Electronic Systems Mag.*, vol. 35, no. 10, pp. 20-28, Oct. 2020.

[10] C.A. Mohr, S.D. Blunt, “Design and generation of stochastically defined, pulsed FM noise waveforms,” *Intl. Radar Conf*., Toulon, France, Sept. 2019.

[11] E.R. Biehl, C.A. Mohr, B. Ravenscroft, S.D. Blunt, "Assessment of constant envelope OFDM as a class of random FM radar waveforms," *IEEE Radar Conf*., Florence, Italy, Sept. 2020.

[12] J. Jakabosky, S. D. Blunt, B. Himed, “Spectral-shape optimized FM noise radar for pulse agility,” *IEEE Radar Conf*., Philadelphia, PA, May 2016.

[13] C. A. Mohr, P. M. McCormick, S. D. Blunt, C. Mott, "Spectrally-efficient FM noise radar waveforms optimized in the logarithmic domain," *IEEE Radar Conf.*, Oklahoma City, OK, Apr. 2018.

[14] B. Ravenscroft, J.W. Owen, J. Jakabosky, S.D. Blunt, A.F. Martone, K.D. Sherbondy, “Experimental demonstration and analysis of cognitive spectrum sensing & notching,” *IET Radar, Sonar & Navigation*, vol. 12, no. 12, pp. 1466-1475, Dec. 2018.

[15] C.A. Mohr, S.D. Blunt, "FM noise waveforms optimized according to a temporal template error (TTE) metric," *IEEE Radar Conf.*, Boston, MA, Apr. 2019.

[16] C.C. Jones, C.A. Mohr, P.M. McCormick, S.D. Blunt, “Complementary FM radar waveforms and optimized receive processing,” to appear in *IET Radar, Sonar & Navigation*.

[17] C.A. Mohr, P.M. McCormick, C.A. Topliff, S.D. Blunt, J.M. Baden, "Gradient-based optimization of PCFM radar waveforms," to appear in *IEEE Trans. Aerospace & Electronic Systems*.

[18] T. Higgins, K. Gerlach, A.K. Shackelford, S.D. Blunt, “Non-identical multiple pulse compression and clutter cancellation," *IEEE Radar Conf.*, Kansas City, MO, May 2011.

[19] H. Griffiths, L. Cohen, S. Watts, E. Mokole, C. Baker, M. Wicks, S. Blunt, "Radar spectrum engineering and management: technical and regulatory issues," *Proc. IEEE*, vol. 103, no. 1, pp. 85-102, Jan. 2015.

[20] A. Parent, M. Morin, P. Lavigne, “Propagation of super-Gaussian field distributions,” *Optical and Quantum Electronics*, vol. 24, no. 9, pp. S1071–S1079, 1992.

[21] S.D. Blunt, E.L. Mokole, “An overview of radar waveform diversity,” *IEEE Aerospace & Electronic Systems Mag*., vol. 31, no. 11, pp. 2-42, Nov. 2016.

[22] A. Papoulis, *Signal Analysis*, Mcgraw-Hill New York, 1984.

[23] E. Ghadimi, R. Feyzmahdavian, M. Johansson, “Global convergence of the heavy-ball method for convex optimization,” *European Control Conf.*, Linz, Austria, July 2015.

[24] J. Nocedal, S. J. Wright, *Nonlinear Equations*, Springer, 2006.

[25] M.A. Richards, J.A. Scheer, W.A. Holm, *Principles of Modern Radar: Basic Principles*, SciTech Publishing, pp. 797-799, 2010.

[26] M.H. Ackroyd, F. Ghani, “Optimum mismatched filters for sidelobe suppression,” *IEEE Trans. Aerospace & Electronic Systems*, vol. AES-9, no. 2, pp. 214-218, Mar. 1973.

[27] A. De Maio, Y. Huang, M. Piezzo, S. Zhang, A. Farina, “Design of radar receive filters optimized according to Lp-norm based criteria,” *IEEE Trans. Signal Processing*, vol. 59, no. 8, pp. 4023-4029, May 2011.

[28] O. Rabaste, L. Savy, “Mismatched filter optimization for radar applications using quadratically constrained quadratic programs,” *IEEE Trans. Aerospace & Electronic Systems*, vol. 51, no. 4, pp. 3107-3122, Oct. 2015.

[29] D. Henke, P. McCormick, S.D. Blunt, T. Higgins, "Practical aspects of optimal mismatch filtering and adaptive pulse compression for FM waveforms," *IEEE Intl. Radar Conf*., Washington, DC, May 2015.